Spring 2014

Nanopowder Synthesis and Characterization of the Natural Superlattice (Bi2)m(Bi2Te3)n for Prospective Thermoelectric Materials

Brian Washburne
John Carroll University, bwashburne14@jcu.edu

Nanopowder Synthesis and Characterization of the Natural Superlattice $(Bi_2)_m(Bi_2Te_3)_n$ for Prospective Thermoelectric Materials

by

Brian Washburne

John Carroll University

Senior Honors Project

Spring, 2014

Abstract

The goal of this study was to synthesize nanocrystals of bismuth telluride (Bi_2Te_3) through scalable bottom-up, wet-chemical methods. Rapid nanocrystal growth is accomplished through microwave stimulation of organically dissolved bismuth and tellurium precursors within the time of one minute. Elemental analysis of our product using Inductively Coupled Plasma Spectroscopy indicated that our samples have excess Bi. Together with structure analysis using Powder X-ray Diffraction, these compounds were found to have Bi:Te ratios of 2:1.

Introduction

With a growing demand for renewable and clean energy sources, the scientific community has been called upon to develop technologies that will realize decreased dependence on traditional energy sources and reduce inefficiencies in current energy consumption. High-efficiency thermoelectric (TE) materials coupled with commercially viable synthesis methods have the potential to greatly impact current energy consumption needs. With this in mind, TE materials have gained significant attention in research.[1-4] However, achieving high-efficiency and low cost TE materials has been a challenge.

The dimensionless figure of merit (*ZT*) is used to measure the efficiency of a material in TE applications. The figure of merit has the following relation

$$ZT = \frac{\alpha^2 \sigma}{\kappa} T \tag{1}$$

where *T* is the temperature, α is the Seebeck coefficient, and σ and κ are electrical and thermal conductivity respectively. Materials with a *ZT* near 1 are interesting for TE applications with a ZT of 3 being sighted as the goal for groundbreaking TE applications.[3] Achieving high *ZT* is often difficult because the a material's electrical and thermal properties are usually unfavorably matched. Materials with a high σ tend to have low α and high κ. This means increasing TE efficiency is a complex problem because an improvement of one parameter may result in a counterproductive change in another parameter. The TE power factor $\alpha^2\sigma$ peaks for carrier concentrations associated with heavily doped semiconductors, a relation that is demonstrated in **Fig. 1**. Carefully controlling the free carriers in a potential TE material is critical in achieving optimal *ZT*.

Another method of interest for optimizing *ZT* is to reduce thermal conductivity through nanostructuring.[1] The total thermal conductivity of a material can be expressed as

$$\kappa = \kappa_e + \kappa_L \tag{2}$$

and is due to thermal conductivity contributions from charge carriers κ_e and lattice vibrations κ_L. Nanostructuring increases the number of grain boundaries effectively limiting the mean free path of lattice vibrations lowering κ_L. This relation can be expressed as

$$\kappa_L = \frac{1}{3} C_v \langle v \rangle \lambda_L \tag{3}$$

were C_v is the molar heat capacity, <*v*> is the mean speed of lattice vibrations, and λ_L is the mean free path of lattice vibrations. Thermal conductivity due to lattice vibrations is the main contributor to thermal conductivity in semiconductors.[1] This relation is also shown in **Fig 1** which demonstrates the potential for a significant improvement in *ZT* with reductions in lattice thermal conductivity.

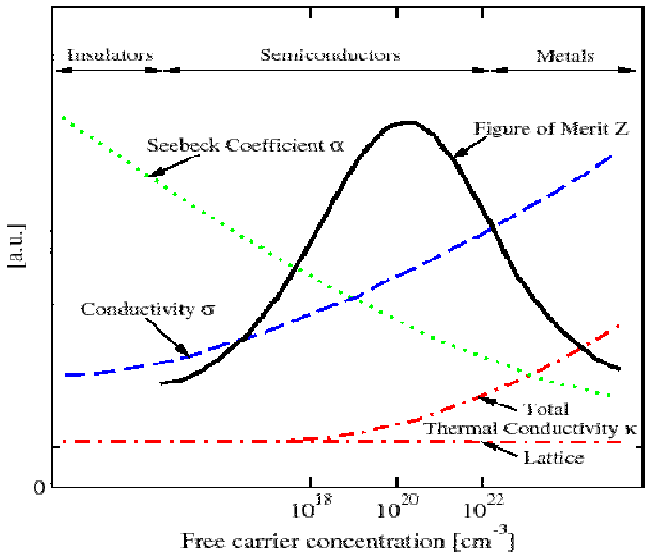

Fig 1. These plots demonstrate how TE transport parameters depend on free carrier concentration.[5] Notice that α peaks for carrier concentrations ~10^{20} cm^{-3}. It can also be seen that κ_L is the primary contributor to κ for semiconductors .

Theory

Nanocrystals of bismuth telluride (Bi_2Te_3) are comprised of hexagonally stacked atomic layers as shown if **Fig 2(a)**. Weak Te-Te bonds contribute to an overall low thermal conductivity. In **Fig 2(b)** it can be seen that Bi_2Te_3 has a high *ZT* near room temperatures compared to other TE materials which make it an attractive material for certain TE applications. It has been shown that high figure of merit Bi_2Te_3 nanocrystals can be produced through scalable bottom-up, wet-chemical methods.[6] Organically dissolved Bi and Te are reacted for one minute through rapid microwave stimulus. Nanostructuring is achieved in this process through size limiting surfactants that are attached to Bi and Te and, near an equilibrium size, shield from further crystal growth. A typical crystal size is 100 nm long and 5 nm wide.[6] These methods are relatively cost effective and time efficient compared to other standard solid-state reaction methods which involve heating of stoichiometric amounts of ground Bi and Te in vacuum sealed quartz tubes for a two week time period.[7]

a.)

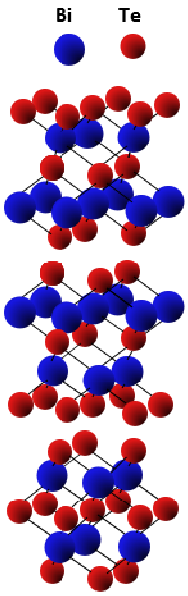

b.)

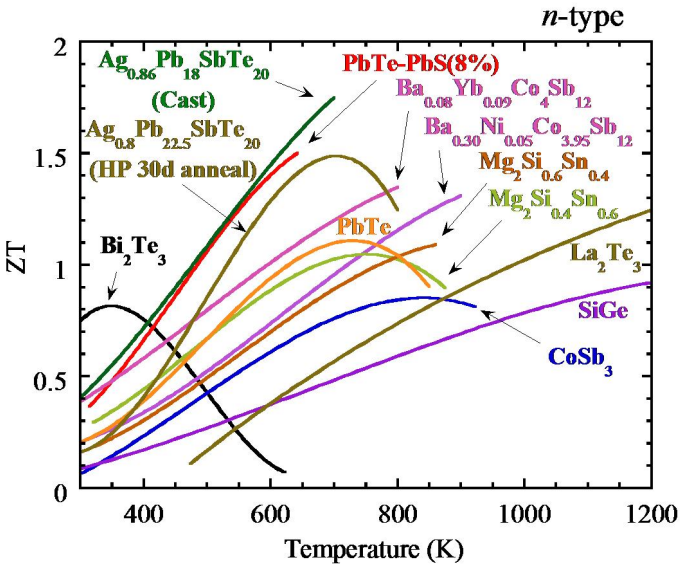

Fig 2. a.) Bi_2Te_3 hexagonally stacked atomic layers with weak Te-Te bonds .b.) Near room temperature *ZT* peaks for Bi_2Te_3.[8]

It has been found that an infinite adaptive series of $(Bi_2)_m(Bi_2Te_3)_n$ exists.[7] Here *m* and *n* are positive integers greater than or equal to zero. This means that blocks Bi_2 and blocks of Bi_2Te_3 can form a compound of any Bi:Te ratio as *m* and *n* vary.

To identify the product resulting from synthesis two analysis methods were used: X-ray diffraction (XRD) and Inductively Coupled Plasma Spectroscopy (ICP). XRD is a powerful technique used to parameterize interatomic structures of crystalline materials. Typical X-ray wavelengths employed in XRD are between 0.1-100 Å. This range is comparable to interatomic distances found in most crystal structures and allows incident X-rays to be diffracted.

The basic operation of an XRD measurement is shown in **Fig 3**. When an X-ray is incident upon a sample crystal structure, atoms within the crystal will cause scattering. At certain angles of incidence constructive interference between X-rays will occur. This relationship is known as Bragg's Law and is shown as

$$n\lambda = 2d\sin\theta \qquad (4)$$

where $n\lambda$ is an integer multiple of the wavelength of an incident X-ray, *d* is the interatomic spacing, and θ is the angle of incidence. A 2θ value is easily obtained as the angle between the Bragg diffracted X-ray, which is reflected by atoms in a material, and the transmitted X-ray that passes through the sample with an unchanged trajectory.

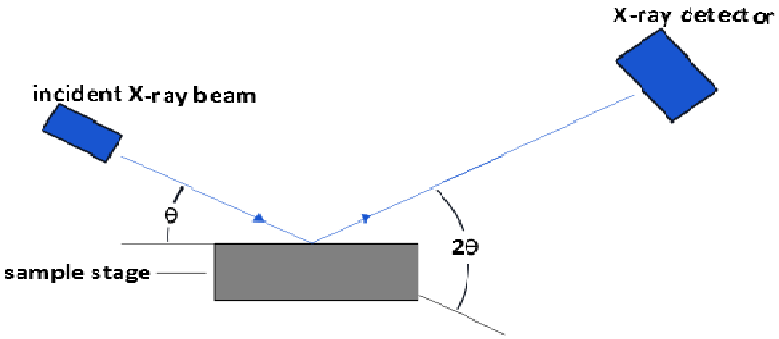

Fig 3. An incident X-ray beam at an angle Θ is reflected into an X-ray detector. An angle of 2 Θ is measured.

Powder diffraction provides constructive interference patterns for all possible orientations of the crystal structure. An XRD pattern is unique to a crystal structure which makes the comparison of a known structure's XRD pattern to an unknown material's XRD pattern useful in identifying an unknown crystal structure.

ICP is a technique used to identify elements within a compound and establish a stoichiometric ratio between identified elements. The ICP measurement is schematically demonstrated in **Fig 4**. A small amount of a sample is typically ingested into concentrated hydro-chloric acid (HCl) which is then diluted to a 4% HCl solution. This solution is then pumped/sprayed into a plasma flame which ionizes the atoms of the sample. When an ionized atom goes from a high energy state to a low energy state, a photon, with a wavelength characteristic of each element, is released. A photon detector measures the intensity of the light emitted due to each of the elements within the sample. These relative intensities are used to establish a stoichiometric ratio between elements in a sample.

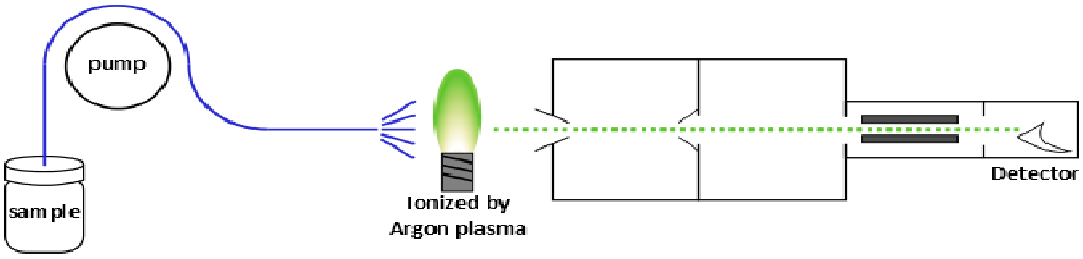

Fig 4. An acidic solution containing an ingested sample is ionized by a plasma flame. Photons are emitted as ionized atoms lower to a ground state. A photon detector measures the intensity of emitted photons.

Experimental

In a small scale synthesis, 0.08 mmol of ground tellurium powder was added to 0.007 mmol of tri-*n*-octylphosphine (TOP) and stirred for 60 minutes resulting in a pale yellow solution. In later synthesis procedures, Te and TOP solutions were microwaved for 4-6 intervals of 80 s producing the same result. Separately, ~0.04 mmol of bismuth chloride ($BiCl_3$) was added to 0.04 mmol of 1,5 pentanediol and then sonicated for ~20 minutes until all visible $BiCl_3$ dissolved into solution. To the $BiCl_3$ and 1,5 pentanediol solution was added 0.004 mmol of TGA; this solution also became pale yellow. The solutions containing dissolved tellurium and bismuth were stirred together for 5 minutes and then microwaved for 60 s in a 1400W domestic microwave oven on high power. During the microwaving a black precipitate formed and a temperature of ~500 K, measured with an inferred thermometer, was reached. The precipitate was then isolated through a cycle of sonication and centrifugation in a Beckman J2-21 at 8000 rpm with 2 washes of isopropanol followed by 2 washes of acetone. During the cleaning process the sample was kept in a 150 mL polypropylene Beckman centrifuge tube. Two scaled up runs were performed following the same procedure, but with ~5x the materials. XRD was performed using a Philips PW 3710 X-ray Diffractometer. ICP was performed using a Perkin Elmer Emission Spectrometer Plasma 400. Commercially purchased Bi and Te standards were used to

prepare a range of Bi and Te ppm solutions with which to correlate the ppm of the Bi and Te to relative intensities from ICP measurements. Both the standards and samples were diluted in 2 % HCl 2% HNO_3 solutions. The weighed samples were digested by stirring for ~24 hours.

Results

Three samples were produced and analyzed using XRD and ICP techniques. **Table 1** shows in mmol the amount of Bi and Te reacted for each of the three samples. The first sample was designed to follow closely a procedures described in literature that was reported to successfully yield Bi_2Te_3 nanocrystals.[6] Samples 2 and 3 were then scaled up ~5x to obtain more precipitate. While samples 2 and 3 did produce more precipitate, the reaction temperatures were lowered by 50°C. This is most likely due to the scaled up samples having a ~5x greater volume compared the volume of sample 1.

Table 1. Three samples were produced, each with the intention of producing Bi_2Te_3. All samples appeared to be Bi rich. Sample 1 was the least Bi rich and had ~5x less Bi and Te going into the reaction.

Sample	Bi (mmol)	Te (mmol)	Molar ratio Bi:Te input	Reaction Temperature (°C)	Molar ratio Bi:Te ICP
1	0.0415	0.0815	1:2	200	2:1
2	0.2850	0.4075	2:3	150	5:2
3	0.2220	0.4075	1:2	150	9:4

XRD for each sample had indistinguishable peak patterns. **Fig 5(a)** shows a representative sample XRD pattern compared to known Bi_2Te and Bi_2Te_3 XRD standards. While the sample XRD pattern has some agreement with both Bi_2Te and Bi_2Te_3 XRD peak patterns, the closest match can be seen to be Bi_2Te. This indicates that our samples have a crystal structure similar to Bi_2Te rather than the Bi_2Te structure.

ICP results shown in **Table 1** were in agreement with XRD, also indicating that all three samples were Bi rich. Samples 1 and 3 had input Bi:Te ratios of 1:2 and sample 2 had an input ratio of 2:3. Despite excess Te in samples 1 and 3, all three samples were found to have Bi:Te ratios close to 2:1. While we expected a Bi:Te ratio of 2:3 for our samples, all ratios of Bi:Te can be understood to fit within the infinitely adaptive series $(Bi_2)_m(Bi_2Te_3)_n$.[7] These results suggest that our sample structure incorporates two Bi_2 blocks between Bi_2Te_3 structures as shown in **Fig 5(b)**. The extent to which Bi_2 blocks are incorporated into a sample's structure could be a function of the amount of Bi going into the reaction. Sample 2, which contained the largest Bi:Te ratio input of 2:3, was found to have the highest Bi:Te ratio of 5:2. Further research directed at exploring the sensitivity of Bi:Te input ratios to resulting Bi:Te output ratios would lead to a better understanding of the control over resulting sample structures possible for this particular synthesis method.

a.) b.)

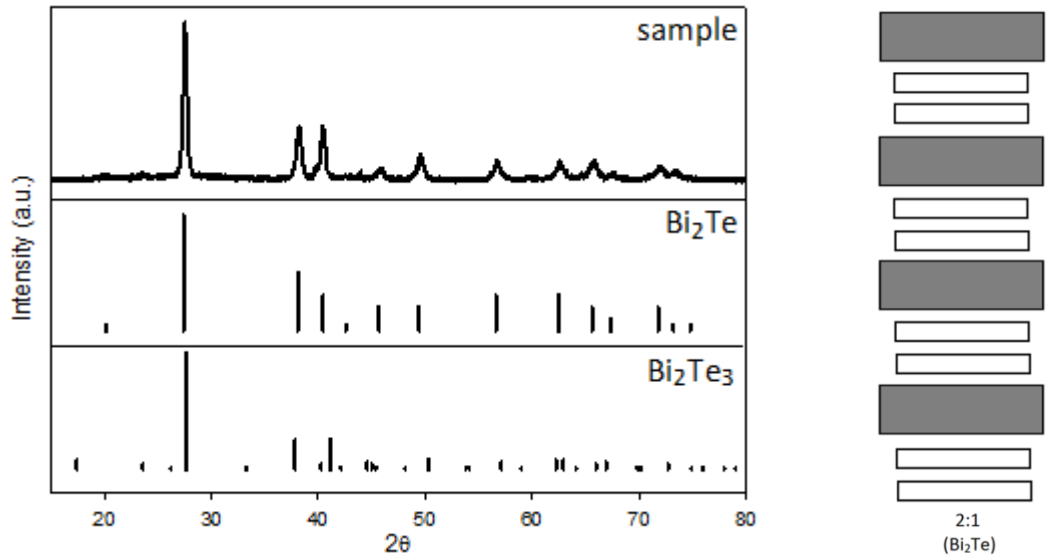

Fig 5. a.) XRD patterns for our sample, Bi_2Te, and Bi_2Te_3. Matching peaks indicates that our samples have a Bi_2Te structure and not a like Bi_2Te_3 structure we had expected. b.) A Bi:Te ratio of 2:1 can be understood to have a supperlattice of Bi_2Te_3 (grey blocks) and Bi_2 (white blocks) as shown.

Conclusion

Reagents of Bi and Te were stimulated via a 60s microwaving interval to initiate rapid nanocrystal growth. Three sample were produced following a set procedure. XRD identified sample's structure to be that of Bi_2Te rather than Bi_2Te_3, and ICP confirmed that samples were Bi rich. Bi rich samples can be understood to incorporate more Bi_2 blocks into a superlattice structure within the infinitely adaptive series $(Bi_2)_m(Bi_2Te_3)_n$.

References

[1]G. S. Nolas, J Sharp, and H. J. Goldsmid, *Thermoelectrics: Basic Prinicples and New Materials Developments*, Springer, Berlin (2001).

[2]D. Rowe, ed., *Thermoelectrics Handbook: Macro to Nano*, CRC Press, Boca Raton (2006).

[3]T. M. Tritt and M. A. Subramanian, "Thermoelectric materials, phenomena, and applications: A bird's eye view," *MRS Bull*. **31**, 188 (2006).

[4]M. Zebarjadi, K. Esfarjani, M. S. Dresselhaus, Z. F. Ren, and G. Chen, "Perspectives on thermoelectrics: from fundamentals to device applications," *Energy Environ*. *Sci*. **5**, 5147 (2012).

[5] Z. Dughaish, "Lead Telluride as a Thermoelectric Material for Thermoelectric Power Generation," *Physica B*, **322**, 205-223 (2002).

[6]R. J. Mehta, Y. Zhang, C. Karthik, B. Singh, R. W. Siegel, T. Borca-Tasciuc, and G. Ramanath, "A new class of doped nanobulk high-figure-of-merit thermoelectrics by scalable bottom-up assembly", *Nature Materials* **11**, 233-24 (2012).

[7]J. W. Bos, H. W. Zandbergen, M.-H. Lee, N. P. Ong, and R.J. Cava, "Structures and thermoelectric properties of the infinitely adaptive series $(Bi_2)_m(Bi_2Te_3)_n$", *Phys. Rev. B* **75**, 195203 (2007).

[8]J. T. Jarman, E. Khalil, and E. Khalaf, "Energy Analyses of Thermoelectric Renewable Energy Sources", *Open Journal of Energy Efficiency* **2**, 143-153 (2013).